metals

Article

Long Sump Life Effects of a Naturally Aged Bio-Ester Oil Emulsion on Tool Wear in Finish Turning a Ni-Based Superalloy

Paul Wood [1], Andrew Mantle [2], Fathi Boud [1], Wayne Carter [1], Urvashi Gunputh [1], Marzena Pawlik [1], Yiling Lu [1], José Díaz-Álvarez [1,3,*] and María Henar Miguélez Garrido [3]

[1] Institute of Innovation in Sustainable Engineering, University of Derby, Kedleston Road, Derby DE22 1GB, UK; p.wood7@derby.ac.uk (P.W.); f.boud@derby.ac.uk (F.B.); w.carter@derby.ac.uk (W.C.); u.gunputh@derby.ac.uk (U.G.); m.pawlik@derby.ac.uk (M.P.); y.lu@derby.ac.uk (Y.L.)
[2] Rolls-Royce Plc, Moor Lane, P.O. Box 31, Derby DE24 8BJ, UK; andrew.mantle@rolls-royce.com
[3] Department of Mechanical Engineering, University Carlos III of Madrid, 28911 Leganés, Spain; mhmiguel@ing.uc3m.es
* Correspondence: j.diazalvarez@derby.ac.uk

Abstract: This paper discusses a method of finish turning Inconel 718 alloy to compare machining performance of a naturally aged and used metalworking fluid (MWF), which had been conventionally managed through its life cycle, with the same new unaged product. The MWF concentrate was a new-to-market bio-ester oil, diluted with water to produce an emulsion. In the experiments, 50 mm diameter bars were turned down with multiple passes at a 250 µm depth of cut to reach a tool flank wear of 200 µm. The machining was interrupted at several stages to measure the flank wear and compare the chip forms for the aged and unaged MWF. The method of finish turning used a small tool nose radius and a small depth of cut that was found to be sensitive in detecting a difference in the flank wear and chip forms for the aged and unaged MWF. On the chemistry, the findings suggest that higher total hardness of the aged MWF was the cause of reduced lubricity and accelerated flank wear. This paper discusses the state of the art with the insights that underpin the finish turning method for the machinability assessment of MWFs. The findings point to stabilization of the MWF chemistry to maintain machining process capability over an extended sump life.

Keywords: machinability; MWF; wear rate; Inconel 718; lubricity; synthetic coolant; coolant aging

check for updates

Citation: Wood, P.; Mantle, A.; Boud, F.; Carter, W.; Gunputh, U.; Pawlik, M.; Lu, Y.; Díaz-Álvarez, J.; Miguélez Garrido, M.H. Long Sump Life Effects of a Naturally Aged Bio-Ester Oil Emulsion on Tool Wear in Finish Turning a Ni-Based Superalloy. *Metals* **2023**, *13*, 1610. https://doi.org/10.3390/met13091610

Academic Editor: Umberto Prisco

Received: 20 July 2023
Revised: 27 August 2023
Accepted: 14 September 2023
Published: 18 September 2023

1. Introduction

Metalworking fluids are used extensively in metalworking processes, such as forming, forging and machining [1–3]. In machining, cutting fluids (CFs) are essential to reduce tool wear and extend tool life and maintain the surface integrity of the part [4–7]. The finish machining of turbomachinery components used in aircraft engines is a critical last stage manufacturing process, and CFs are essential to maintain process capability. Precision-turned parts such as shafts, discs and blisks in aircraft engines account for a high proportion of machined engine components, of which around 50% are made from nickel-based superalloys. At present, the sump life of a well-maintained CF in many industrial applications can be expected to reach a 48-month service life [8].

In use, CFs are exposed to chemical, physical and biological changes over time, which are partly irreversible [2,3,9,10]. CFs degrade due to contamination from the working environment, which reflects in the form of losses in the fluid properties such as flash point, changes in pH and increased foaming [1,11]. CFs therefore require management to mitigate the impact of these effects and to maintain performance within a controlled range.

Emulsion CFs contain typically 90% water which provides a good habitat for the growth of microorganisms, particularly bacteria and fungi [12]. Aerobic bacteria need oxygen for growth; they reproduce by dividing in half approximately every 20 to 30 min [13]. Although there are 30,000 named species of bacteria on earth, there are less than a dozen commonly found in water-miscible fluids [13]. Sulphates in emulsion CFs are particularly detrimental because they promote the growth of a common bacterial species, known for its unpleasant odour [14]. Certain bacteria species can neutralise the chemical ingredients in CFs by reducing the effectiveness of corrosion inhibitors and encourage formation of corrosive organic acids and salts. These not only modify the chemical and physical properties of an emulsion CF but leave sticky residues on machine surfaces and clog filters.

With aging of a CF comes the production of extracellular polymeric substances (EPSs), which is a property of microorganisms in the natural environment. EPSs can lower viscosity [9], decrease pH and increase the mean droplet size in the emulsion. According to [2,3], the aging process can improve the lubricity of the CFs by the presence of certain bacterial species and EPSs, whilst changes in pH have a rather little effect on the lubricity. An increase in a mean droplet size in the CF with age lowers lubricity because it is less effective in penetrating the contact zone between the tool, chip and the workpiece [3].

Inconel 718 alloy belongs to the family of austenitic nickel–chromium (Ni-based) superalloys with mechanical properties suited for high-temperature applications such as gas turbine engine components and heat exchangers [15]. Ni-based superalloys retain their high strength to 650 °C and display high resistance to oxidizing and corrosive environments [15]. As such, Inconel 718 alloy is difficult to machine, with tools displaying high rates of flank and crater wear, chipping and notching, a propensity for BUE and lower productivity compared to many other alloys [5–7,11,16]. In machining Inconel 718, wear is caused by the hard precipitate phases such as γ within the FCC-γ primary phase of the alloy that gradually abrades the tool's cutting edge [17]. Of the different tool failure modes, flank wear is preferred, enabling stable and predictable tool life for process optimization and increased productivity. Industrial machine tools must be stiff for machining high-strength superalloys [7]. Table 1 identifies important published works on turning Inconel 718 [5–7,11,15,18–27] to improve production efficiencies and maintain surface integrity of the machined part by studying a wide range of process parameters, tool geometries and materials, with and without coatings, and coolant types. Of these, only few works [20,21,27] studied finish turning of Inconel 718, using a small tool nose radius of 0.4 mm and a small depth of cut (~0.25 mm) with coated and uncoated tools and an emulsion coolant, and none used a bio-easter emulsion coolant. A small tool nose radius of 0.4 mm and a depth of cut of 0.25 mm are more typical of the tool and process parameters for precision finish turning of Inconel 718 used in industry.

A modern fully synthetic MWF formulated with a vegetable-ester-oil base has been shown to display enhanced lubricity in machining together with a significant reduction in its life-cycle carbon footprint compared to fossil derived MWFs [28]. Other works studied turning of Inconel 718, using graphene nanofluids applied as MQL [29] and vegetable oil [30]. Doped nano-green lubricants in machining Ni-based alloys were studied in [31]. A full review on the application of vegetable oil-based cutting fluids for sustainable machining was undertaken by Kazeem [32]. However, the effect of long sump life on stable machining performance has so far not been previously studied. This paper investigates the functional performance of a vegetable ester oil-based emulsion that was naturally aged through the use in finish turning Inconel 718 bar and compares its machinability with that of the unaged CF. The aged CF was used and maintained in the machine tool with a detailed record kept over a period of 43 months prior to conducting the machinability tests. Through its use life cycle, the aged CF was exposed to an environment typical of a coolant in a machine tool, e.g., particulate contamination, bacterial growth, seasonal temperature and humidity fluctuation and chemistry changes, which can cause a change in the functional properties of the CF over time. The CF was new to market only a few years prior to this study.

Table 1. Performance measures and process parameters studied in published works on turning Inconel 718 alloy.

Speed (mm/min)	Depth of Cut (mm)	Feed (mm/rev)	Tool Nose Radius (mm)	Tool Material	Lubricant Condition	Measures	
30–70	1	0.168–0.393	0.8	TiAlN PVD coated	Dry, vegetable emulsion	Tool wear, surface roughness	[7]
60, 180	0.25	0.1	0.8	Carbide, CBN	Emulsion, dry, cryogenic, CMQL	Tool wear, surface roughness	[23]
50–100	0.4–1.2	0.1–0.2	0.8	Coated carbide	Emulsion	Surface roughness	[11]
45, 90	1	0.2	Tool diameter 12	Carbide	Emulsion	Chip form	[6]
65, 84	0.2, 0.5	0.1	0.8	Uncoated WC	Dry	Tool flank wear, cutting forces, chip form	[24]
100	0.2–0.6	0.12	0.8	Carbide	Dry	Chip form	[15]
60	0.4	0.08–0.2	-	-	Dry and cold air	Surface roughness, XRD analysis	[25]
65–125	0.25	0.1	0.8, 1.2	Carbide	Emulsion	Tool wear	[5]
40–70	0.2–0.8	0.1–0.25	0.8, 1.2	Carbide, ceramic	Emulsion	Cutting force	[26]
30, 80	0.1, 0.5	0.15	0.4	Carbide	Coolant	Residual stress	[27]
60, 120	0.8	0.075	0.8	Uncoated 890 grade carbide	Dry, MQL	Tool wear, cutting forces, surface roughness, chip	[18]
50, 70	0.5	0.1	0.4	Carbide	Dry	Tool wear and surface roughness	[19]
50–300	0.25	0.1–0.15	0.4–0.8	PCBN-Carbide	Emulsion	Forces and surface damage	[20]
40–120	0.25	0.15, 0.25	0.4	K10 coated and uncoated, WC substrate	Emulsion	Residual stress	[21]
30–50	2	0.2–0.4	-	Carbide	Wet	Tool life and forces	[22]

Overview of the Approach Taken

To support the investigation, a method for finish turning the outside diameter of large 50 mm diameter Inconel 718 bar pieces was developed using the aged CF in the machine tool. To complete a full single test cut, the tool is required to reach and exceed the 0.2 mm flank wear. Because a large-diameter bar will be turned down in multiple passes from 50 to 26 mm in diameter, in designing the turning method, it is necessary to ensure that sufficient bar stock is available with a stickout length not exceeding 105 mm from the chuck. A longer stickout would require using tail stock centring for additional support. Using a fixed depth of cut (dc) = 0.25 mm and feed (f) = 0.2 mm/rev appropriate for finish turning, the main cutting surface speed (V) was steadily increased in each of five full test cuts from 40 m/min to 90 m/min. At 90 m/min, the tool flank wear both reached and exceeded 0.2 mm, and the results are displayed in Figure 1a. From these preliminary experiments, V used in the turning method was fixed at 90 m/min.

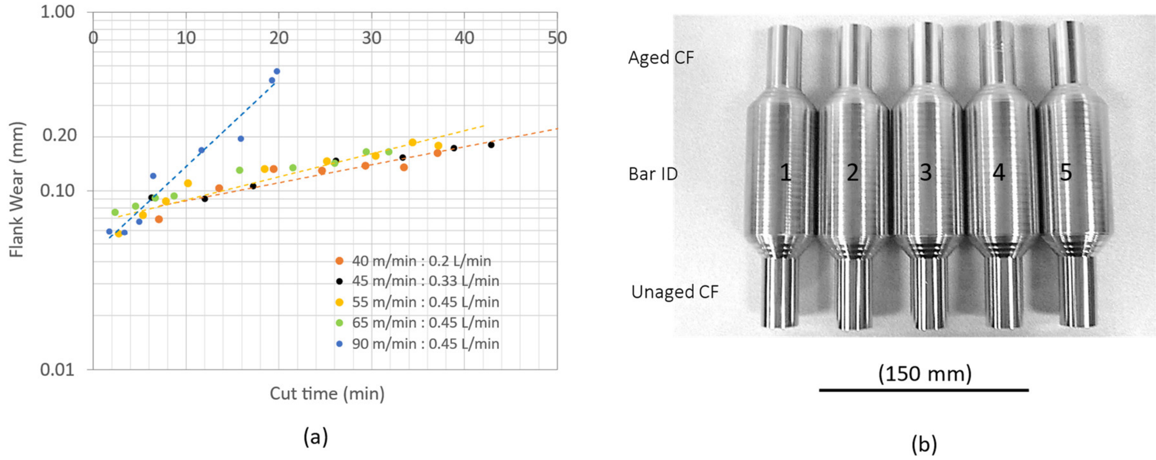

Figure 1. Effect of V on flank wear (**a**) and five bar workpieces each with unique ID to study the aged and unaged CFs (**b**).

For the study described in this paper, five Inconel 718 bars (50 mm diameter × 211 mm length) used for the turning method to compare the wear rate and chip forms were obtained to study the performance of the aged and unaged CFs. The approach taken uses one side of each bar for the aged CF and the other side for the unaged CF as shown in Figure 1b. This way, batch-to-batch variation in mechanical properties of the alloy supplied as bar with standard specification was minimized, and sensitivity to the CF aging effect on the machinability assessment resulting from changes in the physical and chemistry properties was maximized. The five sets of results obtained for the aged and unaged CFs are sufficient to determine statistically significant results.

2. Materials and Methods

2.1. Workpieces

The workpieces used were Inconel 718 bar with nominal 50.8 mm diameter and 211 mm length. The five bar workpieces were obtained from the supplier (BÖHLER, Vienna, Austria) with a mill certificate code G020365000. The bars supplied had been solution-annealed at 1886 °F (1030 °C) for 1.5 h and then age-hardened at 1436 °F (780 °C) for 6.3 h. The mechanical properties of the Inconel 718 bars are given in Table 2 and the composition elements in Table 3. A small flat measuring approximately (mm) 25.5 × 26.5 was machined into the outer diameter of each bar supplied, and the Brinell hardness was measured using an N3200 tester (Innovatest, Halesowen, UK), with indenter 5.0 mm in diameter and test force of 750 Kgf in accord with EN ISO 6506-1:2005 [33]. The hardness was confirmed in the range 339 to 344 HB and in accord with the supplier's certificate. The yield strength of the alloy suggests that the workpieces are in a medium-hard and machinable condition.

Table 2. Mechanical properties of workpiece (Inconel 718) at room temperature.

	Yield Strength (Mpa)	Tensile Strength (Mpa)	Elongation (%)	Reduction in Area (%)	Brinell Hardness
	862–1000	≥1034	≥20	≥35	314–360
ASTM E 23-18 (2018) [34]	889	1220	32	52	341 [1]

[1] ASTM E18-19 (2019) near surface.

Table 3. Chemical composition of Inconel 718 workpiece.

Element	C	Si	Mn	Cr	Mo	Fe	Al	Co	Cu	Ti	Ni	Nb
Wt %	0.014	0.05	0.06	18.9	3.00	18.57	0.53	0.42	0.03	0.95	53.1	5.05

2.2. Machine Tool

A CNC lathe model SLX1630 (XYZ Machine Tools, Tiverton, UK) was used for the experiments and 203 mm chuck diameter type D1-6. The spindle motor was 7.5 HP with a spindle speed range between 150 and 2500 rpm. It had a 42 L coolant tank capacity that was maintained between 25 and 30 L of CF. The coolant pump motor was 1/8 HP that can deliver 25 L/min. The lathe was fitted with a 2 L oil pump to lubricate the slideways, using a mineral oil SW 32 and this was the main source of tramp oil that could contaminate the CF. The lathe was commissioned approximately 43 months prior to the start of these experiments and had only seen light use. For this reason, the oil pump flow rate was at a low setting and dispensed a total quantity not exceeding $\frac{1}{2}$ L over the 43 months (approx. 140 mL per annum) since the machine was commissioned. The chip tray containing tramp oil was wiped clean before and after use and we emphasise that leakage of tramp into the coolant sump was negligible. This was also evidenced by the tramp oil and odour action log record that was monitored by visual inspection, which remained in the target range not requiring any action over the use life cycle.

2.3. Cutting Fluid

The CF for the experiments was a water-miscible synthetic vegetable ester oil-based microemulsion (BLASER, Hasle bei Burgdorf, Switzerland) formulated for long sump life (45-month) and stable with hard water use. The neat concentrate of the CF is a commercially available product, free of mineral oil, chlorine, boron, formaldehyde, bactericides, glycol ether and zinc, and formulated for use with difficult to machine alloys. The water used was main tap water supplied by the local water authority. The recommended hardness for the CF was in the range 15 to 25 °dH (270 to 450 ppm). When diluted with water to form an emulsion, it is semi-transparent. As shown in Figure 2, the CF in the aged condition used in the machine was managed through its use life cycle and inspected at regular intervals with an action log record maintained over a full 43-month period prior to the start of these trials. Over the full 45-month period in use, the pH was maintained at 9.0 with exception to one month (month 18) when it dropped to 8.8; nevertheless, it remained within the ideal target range of 8.8 to 9.5. The concentration level of the neat CF diluted in the water was gradually increased reaching 13% and fixed at this level for the experiments with the aged CF.

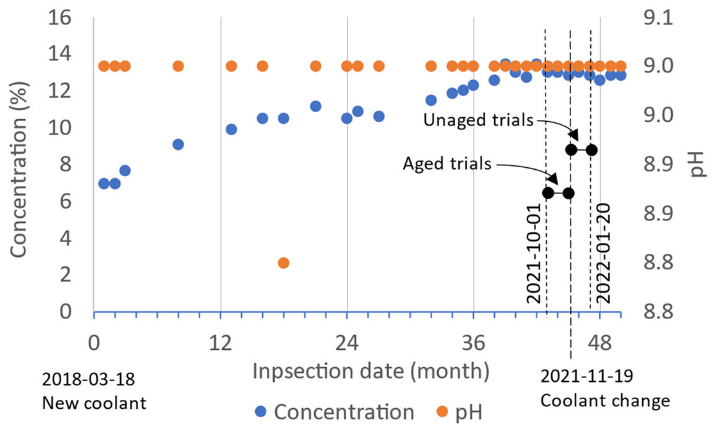

Figure 2. Maintenance record with timeline of aged CF at the start of the experiments.

Immediately before starting a machinability test with each workpiece, the concentration was measured by a refractometer type RHB-32 with range 0–32% Brix in accord with ASTM D3321. The refractometer measurement was multiplied by the CF factor 1.4 to determine the concentration. Adjustment to the CF concentration was made to ensure it was within +/−0.1 of the target concentration. Element analysis of the aged CF samples with concentration at 13% was conducted using inductive coupled plasma (ICP) spectroscopy and microbial count using the dip slide method by an accredited laboratory (PCMS, Rotherham, UK). Analysis of contamination, chemistry and droplet size was performed at the laboratory of the supplier of the CF product. Small samples of the aged CF for analysis in the sump of the machine just before testing started were taken and the condition determined within 24 h after removal. On completing the experiments with the aged coolant over a 1-month period and after 45 months of use, the sump was flushed, cleaned and replaced with the same new unused CF product supplied to the same specification, which will be referred to as the unaged condition. The unaged CF was diluted with main tap water at the same concentration of 13% and further tests were completed within 2 months of changing the coolant. Analysis of the unaged CF samples was performed in the same way at the same laboratories.

2.4. Tool Holder and Tip Insert

The tool holder was supplied by (ISCAR, UK) with designation PWLNR 2525M-06X-JHP Jetcut. The CF was delivered through the tool using a nozzle diameter 2.1 mm. The tip insert (ISCAR, UK) was a double-sided 80° trigon with nominal tool nose radius (R_n) = 0.4 mm made from cemented carbide (WNMG 060404-F3S IC806) and TiALN + AlTiN PVD coated for finish machining hard heat resistant alloys. The tool nose was only partially engaged with depth of cut (dc) set at 0.25 mm and R_n > dc. The tool angle with respect to the round workpiece was −6° negative rake in both feed and radial directions. Similarly, with 6° clearance in feed and radial directions. The small chip breaking feature at the tool edge presents a 14° positive rake over approximately 0.5 mm when mounted in the tool holder. The approach angle used was 95°. Five tip inserts were randomly selected from the batch, and each was measured giving R_n = 0.39 mm with deviation <0.01 mm. The cutting-edge radius on the flat face of the nose was estimated to be between 0.02 and 0.03 mm.

2.5. Set-Up and Method for Experiments

Tool life for precision finish turning was determined by flank wear land (VBz), according to the general definition in ISO 3685 1993E [35]; the subscript (z) denotes the direction of wear, using the coordinate system described in Section 3.1. To measure flank wear rate on the tool, suspending machining at six stages for approximately 30 min was required to take measurements with the final 7th measurement stage after completing the test. For each test cut, the bar workpiece was secured in a 3-jaw chuck with a stickout length 105 mm. Initially, the bar workpiece was lightly skimmed to 50 mm diameter in one pass, using a different tip insert to remove the skin and true the bar on the machine.

2.6. Turning Parameters for This Study

To compare the aged and unaged CFs, the finish turning method used the machining parameters V = 90 m/min, dc = 0.25 mm, f = 0.2 mm/rev and a CF flow rate through the tool of 0.45 l/min with nozzle pressure ahead of the outlet ~0.3 bar. Table 4 identifies the stages and associated cut time to suspend machining to measure flank wear and collect chips. Table 4 also shows the reduction in the bar diameter at the end of each stage, the number of tool passes per stage and the total cut length per stage. At stage 5, the number of tool passes increased from 3 to 12, and the corresponding cut length per stage increased 3.5-fold. The accumulated cut length at the end of stage 7 was 2883 mm (~2.9 m). The tapered shoulder shown in Figure 1b is an intended feature of the machining process design to prevent the tool's leading edge from cutting into the shoulder with each pass that reduces the diameter; otherwise, this could accelerate the tool wear rate.

Table 4. Details of seven measurement stages in turning down each workpiece from a 50 to 26 mm diameter.

Stage Number for Measurement	1	2	3	4	5	6	7
Accumulated cut time (min)	1.75	3.4	4.98	6.48	11.7	16.5	19.3
Number of tool passes per stage	3	3	3	3	12	12	12
Cut length per stage (mm)	206	200	198	194	727	696	662
Nominal bar diameter at start (mm)	50.0	48.5	47.0	45.5	44.0	38.0	32.0
Nominal bar diameter at finish (mm)	48.5	47.0	45.5	44.0	38.0	32.0	26.0

2.7. Instruments

A ShuttlePix P400-R digital microscope (Nikon, Amstelveen, Netherlands) at 150× magnification was used to measure the evolution of flank wear on the tool shown in Figure 3a,b at stages 4 and 6, respectively. Flank wear was measured normal to the major and minor flank straight edges shown by the viewing eyes in Figure 3c. The major flank straight edge was at an angle 5° normal to the feed direction, and similarly, the minor flank straight edge was at an angle 5° normal to the radial direction. The datum 0.0 was at an angle of +45° to the feed direction. The leading edge (LE) extended from 0.0 to the major flank, and the trailing edge (TE) extended from 0.0 to the minor flank. The maximum flank wear (VBz_{max}) shown in Figure 3a,b was measured to a precision of 20 mm. A typical measured flank wear profile around the tool's cutting edge measured on the same tool insert at stages 4, 6 and 7 is shown in Figure 3d.

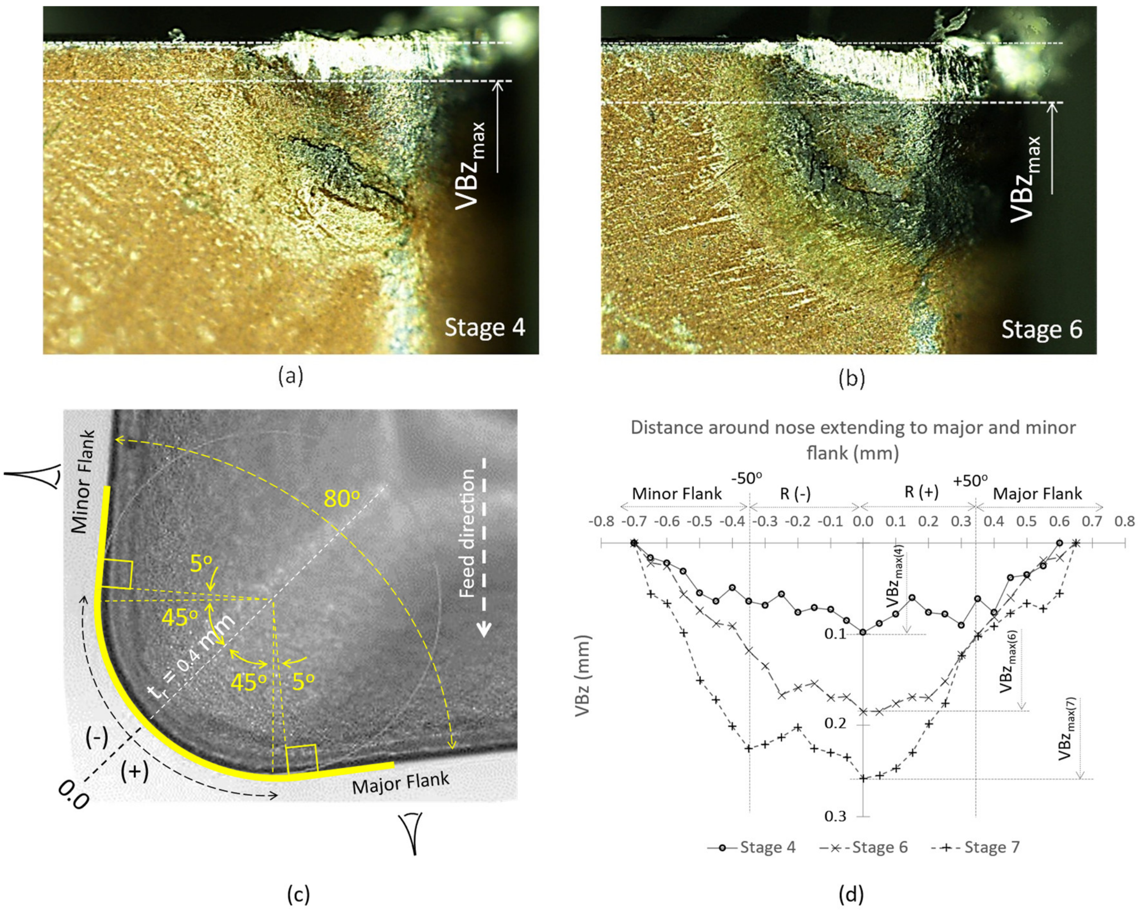

Figure 3. Measurement of flank wear around the tool's cutting edge, using OM flank wear at stage 4 (**a**) and flank wear at stage 6 (**b**); top view of the tool (**c**) and flank wear evolution profile (**d**).

3. Results and Discussion

3.1. Stability of Machine Tool and Workpiece, Using Turning Protocol

According to Rahman [22], chatter vibration is more likely when the radial force in turning increases and especially when the tool insert starts to fail, e.g., at VBz0.2. Using the finish turning method parameters described in Section 2.6, an instrumented turning test was performed with a Kistler type 9119AA2 three-component dynamometer (Kistler, Winterthur, Switzerland) to determine the cutting forces with respect to tool wear. The main cutting force (Fc) is on the *Z*-axis, the feed (or axial) force (Fa) is on the *X*-axis, and radial force (Fr) is on the *Y*-axis. Figure 4a shows the coordinate system with respect to the workpiece. The cutting forces were recorded at each stage together with flank wear VBz_{max} on one bar workpiece. At stage 6, $VBz_{(6)}$ exceeded VBz0.2 attaining 0.262 mm. The cut time (t_c) to VBz0.2 was 12.7 min. Fr increased at a much faster rate than Fc and Fa, confirming higher sensitivity to flank wear, although chatter vibration was not observed in this test.

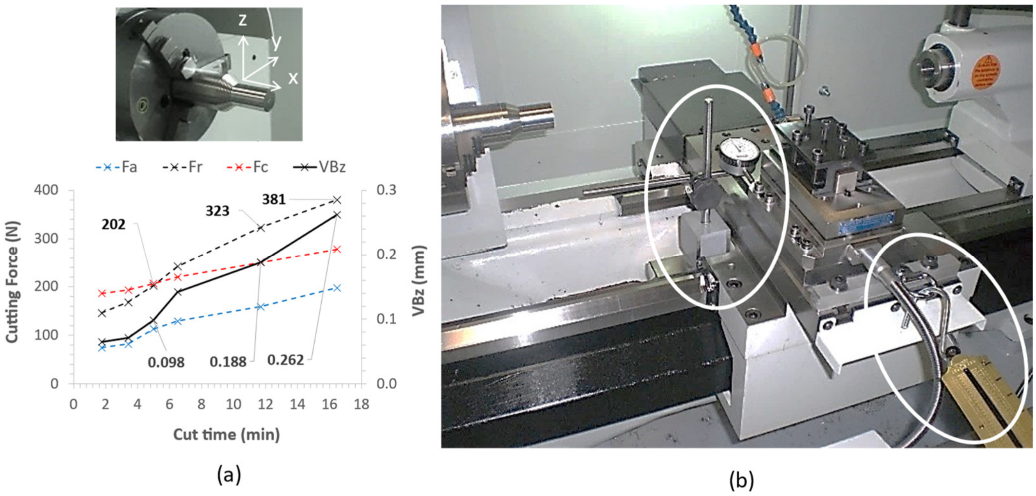

Figure 4. Cutting forces in tangential (Fc), axial (Fa) and radial (Fr) directions with flank wear (**a**) and measurement of machine tool post deflection transverse to main slideway (**b**).

The machine stiffness was checked by applying a tension pull force of 50 kg to the tool post as shown in Figure 4b. Using a dial test indicator (DTI) with a resolution of 2 μm secured to the main slideway, there was no measurable deflection. The same approach was used to check the stiffness of the spindle bearings, applying a pull load of 50 kg with no measurable deflection relative to the main slideway and no play in the spindle bearings. Therefore, the protocol shown in Table 4 was determined to be within the capabilities of the CNC machine tool.

Should a chatter vibration occur as the tool flank wear develops, the cause would most likely be a combination of increased cutting forces (Fr) and reduced workpiece stiffness as the bar diameter is turned down.

Examining the VBz profile and Fr in Figure 4a, the first wear stage of the tool ahead of the characteristic primary region or run-in displays a gradual slow increase in wear with VBz < 0.1 mm, followed by run-in, then a stable wear rate to VBz0.2 and finally a more accelerated wear with loss of tool edge on exceeding VBz0.2.

3.2. Comparing Aged and Unaged Coolant Performance

3.2.1. Flank Wear

Using the finish turning method parameters described in Section 2.6, the evolution of the flank wear for the aged and unaged CFs was measured at the end of each stage, and the results of VBz_{max} for bar piece 1 are shown in Figure 5a.

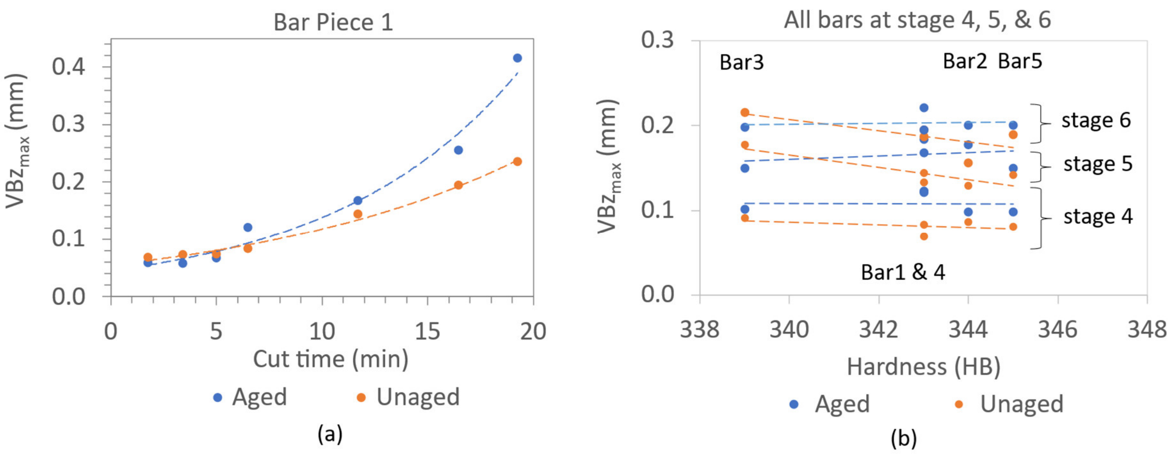

Figure 5. Evolution of flank wear for the aged and unaged CFs (**a**) and effect of material hardness on VBz_{max} at stages 4, 5 and 6 for all bars (**b**).

Figure 5b displays the Vbz_{max} results for the aged and unaged CFs for all five bars at stages 4, 5 and 6 with trend lines fitted. The wear rate results suggest no dependency on bar hardness. We note that the hardness range of the bar stock was low, from 339 to 345 HB. Because the bar stock was supplied with the same batch code, it is probably for this reason the range of hardness was low, and consequently, VBz_{max} did not display dependency on hardness.

Figure 6a displays the difference in the flank wear rate (VBz_{max} diff) between the aged and unaged CFs for all five bars at stages 4, 5, 6 and 7 obtained by subtracting Vbz_{max} for the aged CF from Vbz_{max} for the unaged CF. Stages 1 to 3 were omitted in Figure 6a because they saw little flank wear (VBz_{max} < 0.1 mm) as observed in Figure 5a. Despite the high variability for VBz_{max} diff at stages 5, 6 and 7 in Figure 6a, and to lesser extent at stage 4, most of the VBz_{max} diff results sit on the negative size of the 0.00 flank wear line, with a count of sixteen below and four above, suggesting statistical significance in a qualitative way.

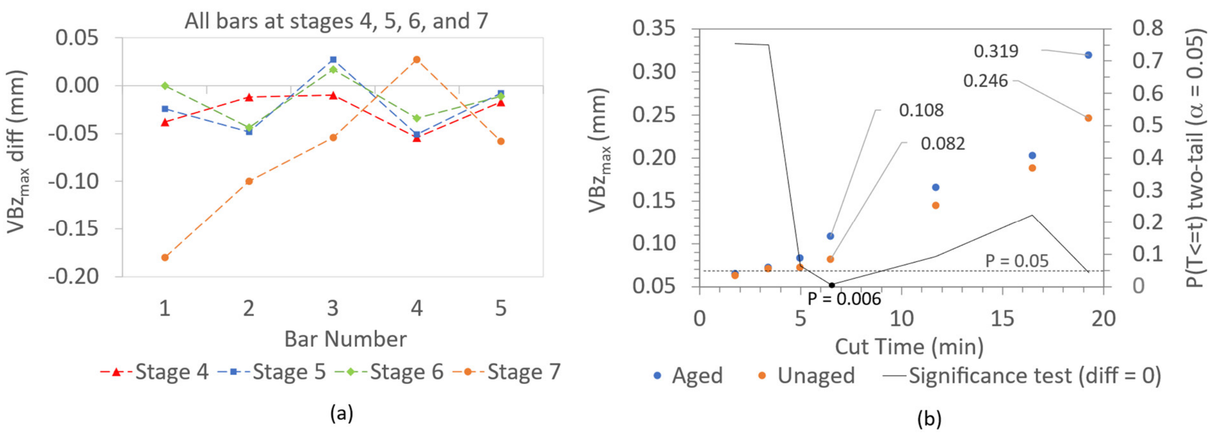

Figure 6. Effect of bar workpiece on VBz_{max} diff (**a**) and average values of VBz_{max} at each measurement stage for the aged and unaged CFs with probability curve (**b**).

With this, it was decided to group the results at each measurement stage obtained from the five different bars. The average value of VBz_{max} with cut time (t_c) determined from five test results for each of the aged and unaged CFs is displayed in Figure 6b. The trend in VBz_{max} with the cut time was described by an empirical exponential growth curve in Equation (1) for t_c => $t_{c(1)}$:

$$VBz_{max}(t_c) = \alpha_1 e^{\alpha_2 t_c} \quad (1)$$

VBz = flank wear rate (μm); t_c = cut time (min); $t_{c(1)}$ = cut time reached at stage 1; α_1 and α_2 are the fitting constants; α_1 is a scaling constant determined from the intercept on the ordinate, and α_2 is a growth rate constant.

Table 5 shows the fitting constants calibrated to the results of the aged and unaged CFs to determine the cut time to reach VBz_{max} = 0.2 mm (VBz0.2). The aged CF displayed a higher flank wear rate with t_c reaching VBz0.2 at 14.7 min compared to the unaged CF with t_c at 17.1 min. The absolute difference in t_c to reach VBz0.2 was 15.1%.

Table 5. Calibrated fitting constants in Equation (1) to determine the cut time (t_c) to reach $VBz_{0.1}$ and $VBz_{0.2}$.

	VBz0.1				VBz0.2			
	α_1	α_2	t_c (min)	Goodness of Fit (R^2)	α_1	α_2	t_c (min)	Goodness of Fit (R^2)
Unaged	51.3	0.0831	8.03	0.87	52.1	0.0787	17.1	0.94
Aged	52.9	0.0987	6.45	0.91	55.7	0.0869	14.7	0.91
Absolute difference (%)			21.8				15.1	

Assuming an unequal variance and a two-tail distribution with 0.05 significance, the probability (P) curve confirms a statistical difference at $t_{c(4)}$ = 6.48 min (stage 4) with P = 0.006. At higher t_c, the rates of flank wear of the aged and unaged CFs converge (stages 5 and 6) until the final stage 7 (t_c = 19.3 min), where they diverge again with P = 0.042. More critical finishing processes require a smaller flank wear limit, e.g., VBz0.1. To determine t_c to reach VBz0.1 with higher accuracy, the fitting constants in Equation (1) were calibrated to the results over stages 1 to 5 and are shown in Table 5. For the unaged CF, t_c was 8.03 min, whilst for the aged CF, t_c was 6.45 min, hence a larger absolute difference in t_c to reach VBz0.1 at 21.8%.

In Figure 7a,b, the tool nose profile is shown at the final stage for both the unaged and aged CFs after machining bar 5. For the unaged CF, the circularity of the tool nose within the tool and the workpiece contact zone that forms the chip is retained, whilst the notch wear appears well-developed for the aged CF.

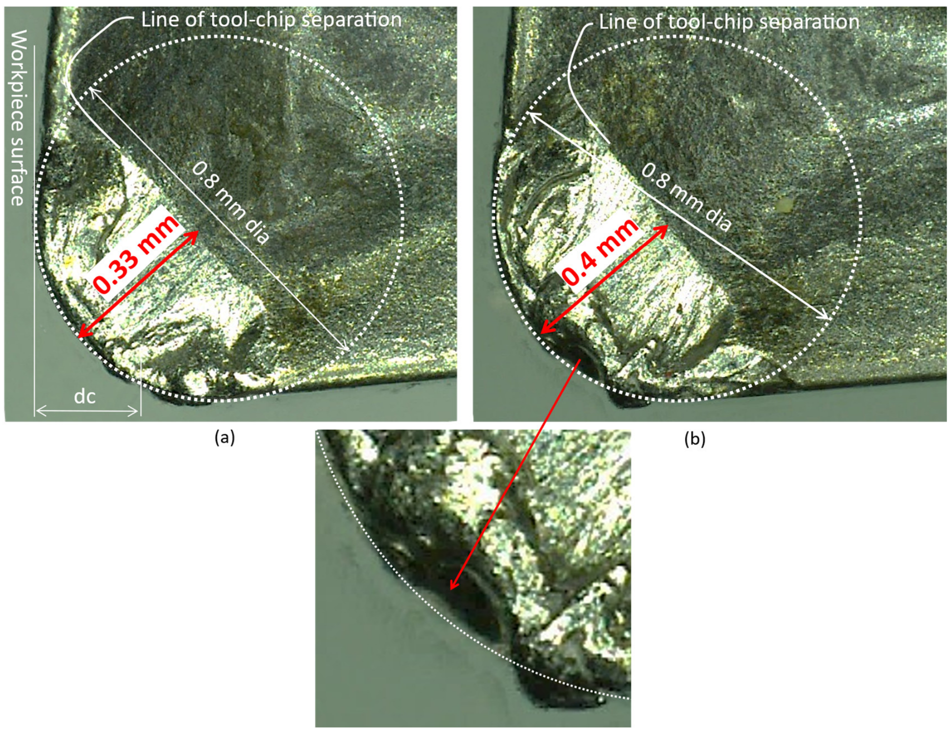

Figure 7. Top view of tool nose after completing stage 7 for the unaged (**a**) and aged CFs (**b**).

3.2.2. Effect of Workpiece Diameter on Tool Flank Wear Measurement

The flank wear on the tool is assumed to be vertical in the *Z*-axis when measured using the OM. In Figure 8, it is observed that the tool wear profile develops an arc between the tool and the workpiece. As bar diameter is reduced with each pass of the tool, the arc of contact also changes. The dimension Y3 is the loss of tool material in the radial direction and is determined from the Equation (2):

$$Y3 = \mathrm{Tan}(\beta)\mathrm{VBz} \tag{2}$$

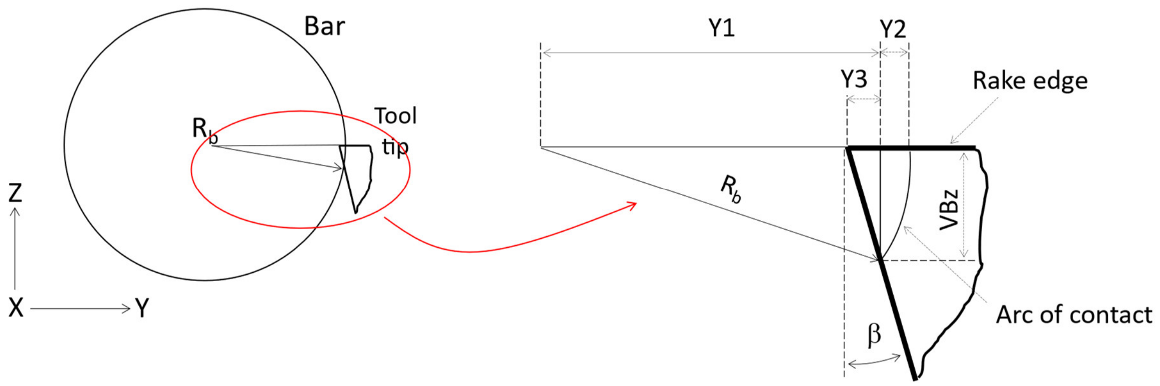

Figure 8. Geometry of tool engagement in workpiece.

Equation (2) assumes that VBz remains vertical in the *Z*-axis with the same coordinate system shown in Figure 4a and a tool clearance angle (β) = 6.

From trigonometry, Y1 and Y2 are determined in Equations (3) and (4):

$$Y1^2 = R_b{}^2 - VBz^2 \tag{3}$$

$$Y2 = R_b - Y1 \tag{4}$$

The effect of the bar diameter on the ratio Y2/Y3 for VBz0.2 is given in Table 6.

Table 6. Effect of bar diameter on the ratio Y2/Y3.

Bar Diameter (mm)	VBz (mm)	Y1 (mm)	Y2 (mm)	Y3 (mm)	Y2/Y3 (%)
100	0.2000	49.9996	0.0004	0.0210	1.9%
50	0.2000	24.9992	0.0008	0.0210	3.8%
26	0.2000	12.9985	0.0015	0.0210	7.3%
10	0.2000	4.9960	0.0040	0.0210	19.0%

As bar diameter reduces from 100 to 10 mm, Y2 increases. However, it is observed that it has more significance when bar diameter reduces below 26 mm. It suggests that more material is lost through wear at the top of the flank than at the bottom of the flank. Figure 9 shows the effect of bar diameter and flank wear limits of VBz0.1 to VBz0.3 on the ratio Y2/Y3. It is observed that the ratio Y2/Y3 increases with the flank wear limit. In Figure 9, the trends of Y2/Y3 for each flank wear limit follow a reciprocal relationship with bar diameter. In the context of the finish turning method described in this paper, Y2 may be considered an error. With a higher flank wear limit, e.g., VBz0.3, it may be desirable to increase the start bar finish diameter to minimize Y2. It is interesting to observe that the flank wear on the turning tool often appears to be tilted slightly inwards as shown in Figure 3a,b.

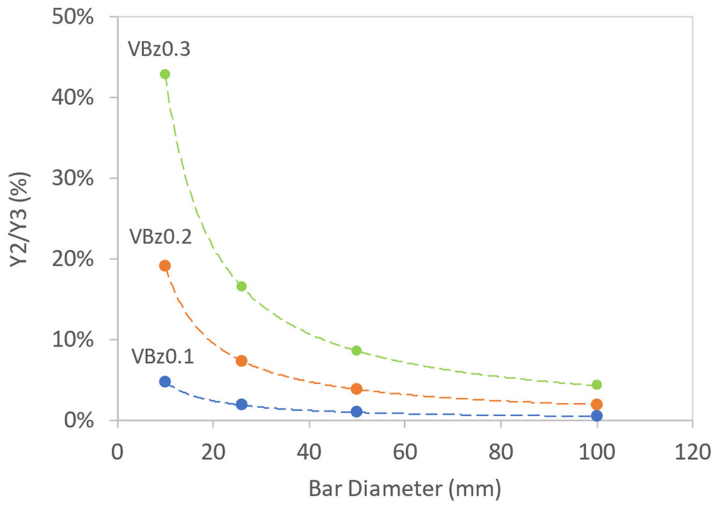

Figure 9. Effect of bar diameter and VBz on the ratio Y2/Y3.

3.2.3. Cutting Forces

A steady increase in main cutting force (Fc) can be seen in Figure 4. According to Altintas [36], this can be explained by an increase in chip friction on the tool rake face from BUE and crater wear, together with ploughing and rubbing edge forces between the tool flank and the workpiece in the tertiary deformation zone. The ploughing edge force is due to the rounding or flattening of the sharp cutting edge, whilst rubbing can be associated with flank wear. On the other hand, the radial force (Fr) and to a lesser extent feed force (Fc) in Figure 4a show the largest relative increase and the trend in Fr correlated with VBz_{max}, confirming a high sensitivity to flank friction and the associated wear rate. Rahman [22] and Yeo [37] drew similar conclusions for turning Inconel 718 with cemented carbide tools. With this, there is confidence that the finish turning method is sensitive to detect changes in MWFs.

3.2.4. Surface Work Hardening

The finish turning of Inconel 718 results in work hardening [25] of the machined surface. The work hardening results in an increase in the surface microhardness of 16%, and although it decreased with depth, its effect was felt up to 125 μm below the turned surface. Surface microhardness was shown to reduce with lower feed rate. We used the same feed rate f = 0.2 mm/rev as in [22]. Assuming the same depth of work hardening, the affected region on the tool is at the leading edge and is concentrated between 0.0 and +45° (see Figure 3c). At 0.0, surface work hardening reduces to zero. In this paper, dc = 0.25 mm, so the tool is cutting 0.125 mm below the work hardened surface. Surface work hardening is expected to increase and deepen with tool wear and could extend further around the profile, between 0.0 and −45°, which is the region that is more likely to affect the precision of the workpiece diameter. In Figure 7b, it is interesting that notch wear for the aged CF was well developed. It is this region of the tool that cuts the workpiece with higher surface and subsurface hardness at the leading edge between 0 and +45° that could accelerate the notch wear.

3.2.5. Chip Forms

Chips obtained from bar 4 at stages 1, 4 and 6 are displayed in Figure 10. In all tests, BUE was seen to develop at stage 2. According to ISO 3685-1993 (E) [35], the chip forms at stage 1 are long helical chips. Chip curl develops because chip velocity increases as uncut chip thickness reduces from LE to TE. The chip flow direction was a right-hand helix in the direction of feed motion and away from the workpiece until the chip became entangled in later wear stages. At stage 1, the helix pitch and radius were slightly larger for the aged CF. For the unaged CF, the chip flow direction according to the classification by

Nakayama [38] was positive up-curl with a positive chip flow angle relative to the line of tool–chip separation defined by Colwell [39] as shown in Figure 7. For the aged CF, the chip flow was similar but with more positive side-curl. More side-curl could be associated with reduced lubricity because it restricts the flow of chip that would otherwise occur at the free edge with more effective lubrication. The helix on the chip form of the aged CF was lost at stage 4, and we note that the statistical difference in flank wear between the aged and unaged CFs was most significant at this stage. The change in the chip form of the aged CF could be associated with the start of crater wear at VBz0.1.

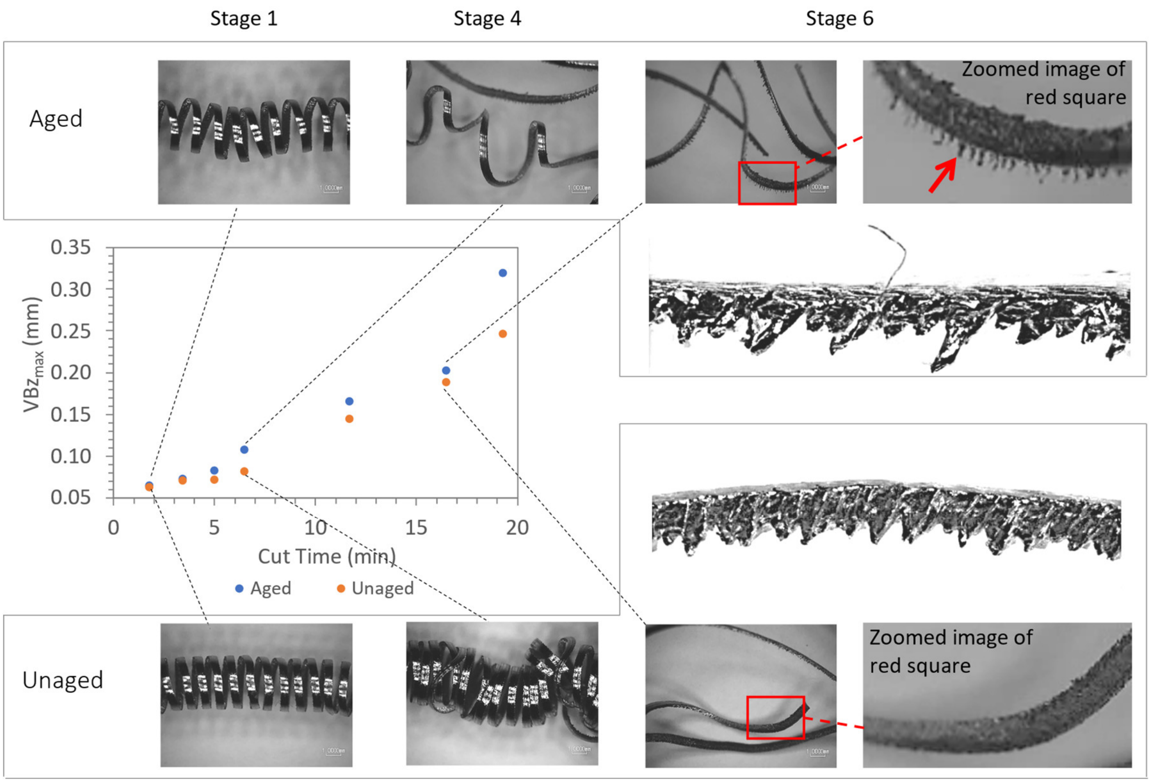

Figure 10. Chips from bar 4 and associated flank wear at stages 1, 4 and 6.

At stage 6, long-snarled ribbon chips developed in all tests with the aged CF, whilst for the unaged CF, three of the five test results had this chip form. Long-snarled ribbon chips retained positive side-curl because the chip continued to flow in the direction of feed motion and away from the workpiece. Due to the increased contact area between the chip and the tool rake face, this chip form is expected to accelerate the flank and crater wear. For the aged CF, irregular serrated saw tooth features are prominent along the chip at stage 6, whilst the unaged CF displays more consistent periodic serrations similar to those obtained by Tamil [6] and Rakish [15] in machining Inconel 718. The irregular saw tooth features could be attributed to vibration. At stage 6, in the zoomed image of the red square, feathering along one edge of the aged CF highlighted by the red arrow was seen to develop on reaching VBz0.2. The incidence of chip entanglement (CE) for the aged CF was present in three tests at stage 6, whilst it was not observed for the unaged CF. At stage 7, CE was present in all aged CF chips and was only present in three tests for the unaged CF. In precision finish turning, if chip form is the main consideration, the flank wear limit of VBz0.1 may apply. Otherwise, VBz0.2 may be a practical upper limit for the parameters used in this study. Although V has a significant effect on the developed chip form [23,40,41], Figure 10 suggests that lubricity is important in maintaining a good chip form.

3.2.6. Temperature

Using a thermocouple welded to the cutting tool, Boud [42] studied the effect of bar diameter on cutting temperature with V fixed at 10, 20, 30 and 40 m/min, using three bars sizes similar to the range of turned diameters used in this paper. It was found that the tool temperature increased in turning a smaller diameter bar and the difference was greater at higher V. According to [22], tool life decreases at higher V because more heat is generated. In this study, V was higher at 90 m/min than the tool supplier recommended parameters, and the workpiece diameter was turned down from 50 to 26 mm in each test to obtain VBz0.2. The aged and unaged CFs were diluted in the same ratio of neat concentrate to water, so their cooling effectiveness in use is unlikely to differ. Instead, the most likely cause of the higher wear rate in the early stages with VBz < 100 µm could be attributed to the reduced lubricity of the aged CF. This is supported by the findings at the end of stage 4 where the unaged CF displayed reduced flank wear and maintained a good chip form. Beyond stage 4, the difference in the flank wear shown in Figure 6b reduced at stages 5 and 6 as VBz0.2 was approached, and we note that the bar diameter reduced to 38 mm at stage 6. With the advancement of both flank and crater wear, temperature may be exerting a stronger effect on the tool wear rate over lubricity beyond stage 4, and it was noted that there was one instance of the tool nose glowing red due to high temperature on reaching VBz0.3. In other works [41] on turning Inconel 718, friction over a very short cut duration to mitigate the effect of tool wear was studied using a semisynthetic petroleum-based emulsion CF [43] diluted with water at a lower concentration (7%) and compared with a dry-cut condition. The V was varied between 60 and 120 m/min, and similar feed was used as described in this paper, but the CF was found to deliver no practical benefit in reducing friction.

4. Analysis of Coolant Samples

4.1. Element Analysis

The results of the element analysis indicated that small trace elements of aluminium and copper were present in the aged CF because light machining of alloys containing these elements was carried out over the 43-month period preceding this experiment. The total volume of dissolved elements was marginally higher in the unaged CF (211 ppm) than in the aged CF (80.9 ppm).

4.2. Contamination

In Table 7, the ferrous content given by the FW wear index was 13.2 and 13.0 for the aged and unaged CFs, respectively, with both classified as a low-fault level not requiring any action. The appearance of the aged and unaged CFs displayed fine dispersion in the emulsion, although the colour of the aged CF was brownish, whilst for the unaged CF, it was slightly yellowish.

Table 7. Analysis of the aged and unaged CF samples.

	Test	Unit	Limits	Unaged	Aged
Contamination	FW index	Comparative		13.2	13
	Colour			Yellowish	Brownish
	Emulsion condition			Fine dispersion	Fine dispersion
Chemistry	pH		8.7–9.3	9	8.9
	Conductivity	mS/cm	<7.0	4.7	4.6
	Nitrate	mg/L	<150	8	26
	Total hardness	°dH	<70	11	19
	Chloride	mg/L	<150	57	84
	Sulphate	mg/L	<400	111	200
Supplementary	Average droplet size	µm	<0.700	0.122	0.113

4.3. Chemistry

Table 7 shows that the total hardness of the aged CF sample was 19 °dH (339 ppm), whilst the unaged CF sample was 11 °dH (196 ppm). CFs prepared from softer water are more stable taking much longer for the salt and mineral contents to separate out of the emulsion [44]. With low water hardness, foaming can occur, resulting in lower tool life and poor surface finish [45]. Conversely, higher water hardness causes a variation in the emulsion droplet size through the lack of stability [45,46], which can affect lubricity. Emulsion CFs work more effectively with the droplet size below 1.5 µm [47]. The average droplet size for the aged and unaged CFs was 0.113 and 0.122 µm, respectively, and the measured difference between them was small. This small droplet size is well below 1.5 µm and more typical of a true solution. The authors of [44] used a linear reciprocating tribometer to show quantitively that lubricity reduces with increasing water hardness of an emulsion CF. Although the contact pressure at 0.3 MPa and velocity range up to 2 m/min in this study were quite low, it could explain the improved lubricity of the unaged CF with lower total hardness. A CF in use could be softened with the addition of additives or the concentrate dilution ratio adjusted to maintain total hardness within a desirable range.

4.4. Microorganism Effects

The dissolved minerals and salts in the CF determine the acidity. The pH of the unaged CF was 9.0, whilst for the aged CF, it was 8.9. Ideally, coolants should have a pH value between 8.8 and 9.2 [44]. For a long-service-life coolant, the pH range should fall between 7 and 9 [48], and the former is neutral, although the range 8.5 to 11 could be acceptable. The pH record of the aged CF was stable at 9.0 as shown in Figure 2, suggesting that the CF was well-managed for long service life. The bacteria count was below the minimum threshold of detection using the dip slide method in the aged and unaged CFs. The nitrate level, which is an indicator of microbial activity, was low in the aged and unaged CF samples, at 26 and 8 mg/L, respectively, being well below the recommended limit of 150 mg/L.

4.5. Nonwater Hardening Ions

The sulphate content in the aged and unaged CFs was 200 and 111 mg/L, respectively, whilst the chloride content was 84 and 57 mg/L. Even at low levels, chlorides and sulphates can cause corrosion because the presence of ions in an electrolyte such as chlorides and sulphates contributes to galvanic corrosion in metals [45]. Both measures were below their respective recommended upper control limits. It has been reported that the chloride and sulphate levels should be kept below 150 ppm which is equivalent to 150 mg/L calcium carbonate [49]; otherwise, these ions can begin to affect the functionality of the coolant, and this may have occurred in the aged CF.

The increased corrosivity of a coolant can be measured by an increase in electrical conductivity resulting from a higher level of dissolved ions in the coolant [50]. It is noted that in high purity or distilled water, the electrical charge cannot flow, because there are no impurities and therefore no ions. The electrical conductivity of the aged and unaged coolants was 4.6 and 4.7 mS/cm, respectively, which appears to contradict the sulphate and chloride measurements. However, the measured difference is very small and well below the recommended upper limit of 7 mS/cm.

5. Conclusions

Comparing the naturally aged-through-use and managed CF and the unaged CF, the method of finish turning Inconel 718 alloy with a small tool nose radius and small depth of cut was shown to be sensitive in detecting a difference in performance. The trends observed for the flank wear and chip forms suggest that the method was stable and reproducible for the machinability assessment of MWFs. The effect of the difference in the CF condition on these measures was most significant for the cut time to reach the lower flank wear limit VBz = 100 µm. For the aged CF, the absolute difference was 21.8% lower and was attributed to reduced lubricity. In this region, the flank wear was dominant because a good chip form was maintained. Beyond VBz > 100 µm, it is unclear if increased flank or crater wear was responsible for the loss of a good helical chip form because the rake face was hidden by the BUE. Because the chips changed to a snarled form going beyond VBz > 100 µm, we think that crater wear may have been the cause. Beyond VBz > 200 µm, collapse of the top edge of the tip ensued. With VBz > 100 µm, the difference in the cut time between the aged and unaged CFs to reach VBz = 200 µm was reduced to 15.1% absolute difference, and the evidence suggests that cooling had a more significant role.

On the chemistry, the findings point to higher total hardness of the CF as the main cause of reduced lubricity of a synthetic vegetable-ester-oil emulsion in machining. Contamination by the ferrous content, dissolved solids and microbial activity was thought to have had a minor role in influencing the lubricity. From a practitioner's perspective, it was also noted that no sticky deposits from the use of the bio-easter oil-based CF in either the aged or unaged condition remained on the machine tool's slideways.

The key findings of the method of finish turning for the assessment of MWFs, using a small tool nose radius and a small depth of cut, discussed in this paper are summarized as follows:

- The flank wear profile was shown to be the maximum on the tool nose midway between the major and minor flank edges.
- The measured radial force (Fr) on the tool increased at a much faster rate than the main cutting (Fc) and feed (Fa) forces, confirming a higher sensitivity to the flank wear. Moreover, the nonlinear trend in the flank wear before VBz_{max} stabilised correlated well with Fr.
- The measured wear rate results were unable to show dependency on the bar hardness, which was attributed to the low hardness range of the bar stock from 339 to 344 HB, which was sourced from a single batch.
- Although the aged and unaged CFs were tested on the same bar piece, there was high variability in the difference in the flank wear between the aged and unaged CFs. Nevertheless, there was confidence that the flank wear for the aged CF suggested reduced performance in a qualitative way. Consequently, the wear results obtained from the five different bars for the aged CF were grouped at each measurement stage, and similarly for the unaged CF, enabling a quantitative statistical comparison of the wear results at each stage.
- Irregular saw tooth features on a chip form obtained from the aged CF on reaching VBz0.2 could be attributed to vibration. Feathering along one edge was also visible for the aged CF on reaching VBz0.2 and could be attributed to the reduced lubricity of the aged CF.
- The flank wear on the turning tool which often appears to be tilted slightly inwards was explained by the arc of contact that develops between the bar diameter and the flank wear on the tool. More material is lost through the wear at the top of the flank than at the bottom of the flank, and it was shown that the smaller the bar diameter, the greater the difference. This could explain the findings of Boud [42] who found that the tool temperature increased in turning a smaller diameter bar at the same surface-cutting speed.
- Turning down the bar workpiece with multiple passes of the cutting tool at a small depth of cut could accelerate the notch wear at the leading edge of the tool as shown for the aged CF, which could be attributed to higher surface and subsurface hardness that develops on the workpiece through reduced lubricity.

Author Contributions: Conceptualization, P.W., A.M. and J.D.-Á.; methodology, A.M., W.C. and P.W.; validation, A.M., M.H.M.G., F.B. and U.G.; formal analysis, A.M., P.W. and F.B.; investigation, W.C., P.W. and M.P.; resources, M.P. and Y.L.; data curation, F.B., M.P. and U.G.; writing—original draft preparation, P.W., A.M., J.D.-Á. and F.B.; writing—review and editing, A.M., M.H.M.G., P.W., U.G. and Y.L.; visualization, J.D.-Á. and Y.L.; supervision, A.M.; project administration, P.W. All authors have read and agreed to the published version of the manuscript.

Funding: This project was funded by Rolls-Royce, project number CFA IN718 (91591), and the development of the paper was funded by the University of Derby's College of Science and Engineering and UC3m in Madrid.

Data Availability Statement: The data are unavailable due to privacy and therefore remains confidential.

Acknowledgments: Rolls-Royce plc for providing guidance on the development of this paper.

Conflicts of Interest: The authors declare no conflict of interest.

Abbreviations

BUE	Built-up edge
CE	Chip entanglement
CF	Cutting fluid
X, Y, Z	Axes of global coordinate system
Fc (N)	Main cutting force on *Z*-axis
Fa (N)	Axial force on *X*-axis
Fr (N)	Radial force on *Y*-axis
dc	Depth of cut (mm)
f	Feed rate (mm/rev)
R_n	Tool nose radius (mm)
t_c	Cut time
V	Cutting surface speed (mm/min)
LE	Tool leading edge
TE	Tool trailing edge
PPM	Parts per million
R_b	Bar workpiece radius
VBz	Tool flank wear
VBz0.1	Flank wear limit 0.1 mm
VBz0.2	Flank wear limit 0.2 mm
VBz0.3	Flank wear limit 0.3 mm
VBz_{max}	Maximum flank wear measured on tool nose
VBz_{max}diff	Flank wear difference [VBz_{max} (unaged CF) − Vbz_{max} (aged CF)]
Y3	Loss of tool material from flank wear in the radial direction
(n)	Stage number to suspend job and measure flank wear
β	Tool tip clearance angle
$k_{1,2}$	Constants in equations.

References

1. Brinksmeier, E.; Meyer, D.; Huesmann-Cordes, A.G.; Herrmann, C. Metalworking fluids—Mechanisms and performance. *CIRP Ann.—Manuf. Technol.* **2015**, *64*, 605–628. [CrossRef]
2. Seidel, B.; Meyer, D. Investigation of the influence of aging on the lubricity of metalworking fluids by means of design of experiment. *Lubricants* **2019**, *7*, 94. [CrossRef]
3. Seidel, B.; Meyer, D. Influence of artificial aging on the lubricating ability of water miscible metalworking fluids. *Prod. Eng.* **2019**, *13*, 425–435. [CrossRef]
4. Derani, M.N.; Ratnam, M.M. The use of tool flank wear and average roughness in assessing effectiveness of vegetable oils as cutting fluids during turning—A critical review. *Int. J. Adv. Manuf. Technol.* **2021**, *112*, 1841–1871. [CrossRef]
5. Grzesik, W.; Niesłony, P.; Habrat, W.; Sieniawski, J.; Laskowski, P. Investigation of tool wear in the turning of Inconel 718 superalloy in terms of process performance and productivity enhancement. *Tribol. Int.* **2018**, *118*, 337–346. [CrossRef]
6. Tamil Alagan, N.; Zeman, P.; Mara, V.; Beno, T.; Wretland, A. High-pressure flank cooling and chip morphology in turning Alloy 718. *CIRP J. Manuf. Sci. Technol.* **2021**, *35*, 659–674. [CrossRef]
7. Saleem, M.Q.; Mehmood, A. Eco-friendly precision turning of superalloy Inconel 718 using MQL based vegetable oils: Tool wear and surface integrity evaluation. *J. Manuf. Process.* **2022**, *73*, 112–127. [CrossRef]
8. Cutting Oil-Water Soluble Cutting Oil Manufacturer from Mumbai. Available online: https://www.dnrcorporation.in/cutting-oil.html (accessed on 25 August 2023).
9. Kavita, K.; Singh, V.K.; Mishra, A.; Jha, B. Characterisation and anti-biofilm activity of extracellular polymeric substances from Oceanobacillus iheyensis. *Carbohydr. Polym.* **2014**, *101*, 29–35. [CrossRef]
10. Rabenstein, A.; Koch, T.; Remesch, M.; Brinksmeier, E.; Kuever, J. Microbial degradation of water miscible metal working fluids. *Int. Biodeterior. Biodegrad.* **2009**, *63*, 1023–1029. [CrossRef]

11. Sivalingam, V.; Zhao, Y.; Thulasiram, R.; Sun, J. Machining Behaviour, surface integrity and tool wear analysis in environment friendly turning of Inconel 718 alloy. *Measurement* **2021**, *174*, 109028. [CrossRef]
12. Koch, T.; Passman, F.; Rabenstein, A. Comparative study of microbiological monitoring of water-miscible metalworking fluids. *Int. Biodeterior. Biodegrad.* **2015**, *98*, 19–25. [CrossRef]
13. Bulletin, T. *Background on Bacteria and Fungus in Metalworking Fluids*; Perrysburg, OH, USA. 2006. Available online: https://www.masterfluids.com/na/en-us/technical-information/technical-bulletins.php (accessed on 17 September 2023).
14. Institute of Advanced Manufacturing Sciences. *Pollution Prevention Guide to Using Metal Removal Fluids in Machining Operations*; Institute of Advanced Manufacturing Sciences: Cincinnati, OH, USA, 1995.
15. Rakesh, M.; Datta, S.; Sankar, S. ScienceDirect Effects of Depth of Cut during Machining of Inconel 718 using Uncoated WC Tool. *Mater. Today Proc.* **2019**, *18*, 3667–3675. [CrossRef]
16. Darshan, C.; Jain, S.; Dogra, M.; Gupta, M.K.; Mia, M.; Haque, R. Correction to: Influence of dry and solid lubricant-assisted MQL cooling conditions on the machinability of Inconel 718 alloy with textured tool. *Int. J. Adv. Manuf. Technol.* **2019**, *105*, 1835–1849, Erratum in *Int. J. Adv. Manuf. Technol.* **2019**, *105*, 1851. [CrossRef]
17. Mahadevan, S.; Nalawade, S.; Singh, J.B.; Verma, A.; Paul, B.; Ramaswamy, K. Evolution of δ phase microstructure in alloy 718. In Proceedings of the 7th International Symposium on Superalloy, Pittsburgh, PA, USA, 10–13 October 2010; Volume 718, pp. 737–750.
18. Kaynak, Y. Evaluation of machining performance in cryogenic machining of Inconel 718 and comparison with dry and MQL machining. *Int. J. Adv. Manuf. Technol.* **2014**, *72*, 919–933. [CrossRef]
19. Cantero, J.L.; Díaz-Álvarez, J.; Miguélez, M.H.; Marín, N.C. Analysis of tool wear patterns in finishing turning of Inconel 718. *Wear* **2013**, *297*, 885–894. [CrossRef]
20. Criado, V.; Díaz-Álvarez, J.; Cantero, J.L.; Miguélez, M.H. Study of the performance of PCBN and carbide tools in finishing machining of Inconel 718 with cutting fluid at conventional pressures. *Procedia CIRP* **2018**, *77*, 634–637. [CrossRef]
21. Sharman, A.R.C.; Hughes, J.I.; Ridgway, K. An analysis of the residual stresses generated in Inconel 718 TM when turning. *Mater. Process. Technol.* **2006**, *173*, 359–367. [CrossRef]
22. Rahman, M.; Teo, T.T.; Ridge, K. The Machinability of Incone1 718. *J. Mater. Process. Technol.* **1997**, *36*, 199–204. [CrossRef]
23. Ostrowicki, N.; Kaim, A.; Gross, D.; Hanenkamp, N. Effect of various cooling lubricant strategies on turning Inconel 718 with different cutting materials. *Procedia CIRP* **2021**, *101*, 350–353. [CrossRef]
24. Thrinadh, J.; Mohapatra, A.; Datta, S.; Masanta, M. Machining behavior of Inconel 718 superalloy: Effects of cutting speed and depth of cut. *Mater. Today Proc.* **2019**, *26*, 200–208. [CrossRef]
25. Kaynak, Y.; Tascioglu, E. Finish machining-induced surface roughness, microhardness and XRD analysis of selective laser melted Inconel 718 alloy. *Procedia CIRP* **2018**, *71*, 500–504. [CrossRef]
26. Yao, C.; Zhou, Z.; Zhang, J.; Wu, D.; Tan, L. Experimental study on cutting force of face-turning Inconel 718 with ceramic tools and carbide tools. *Adv. Mech. Eng.* **2017**, *9*, 1–9. [CrossRef]
27. Madariaga, A.; Kortabarria, A.; Hormaetxe, E.; Garay, A.; Arrazola, P.J. Influence of tool wear on residual stresses when turning Inconel 718. *Procedia CIRP* **2016**, *45*, 267–270. [CrossRef]
28. Wood, P.; Boud, F.; Carter, W.; Varasteh, H.; Gunputh, U.; Pawlik, M.; Clementson, J.; Lu, Y.; Hossain, S.; Broderick, M.; et al. On the lubricity and comparative life cycle of biobased synthetic and mineral oil emulsions in machining Titanium Ti-6Al-4V at low cutting speed Sensitivity: Internal. *J. Manuf. Mater. Process.* **2022**, *6*, 154. [CrossRef]
29. Gong, L.; Bertolini, R.; Ghiotti, A.; He, N.; Bruschi, S. Sustainable turning of Inconel 718 nickel alloy using MQL strategy based on graphene nanofluids. *Int. J. Adv. Manuf. Technol.* **2020**, *108*, 3159–3174. [CrossRef]
30. Teo, J.J.; Olugu, E.U.; Yeap, S.P.; Abdelrhman, A.M.; Aja, O.C. Turning of Inconel 718 using Nano-Particle based vegetable oils. *Mater. Today Proc.* **2020**, *48*, 866–870. [CrossRef]
31. Sen, B.; Mia, M.; Mandal, U.K.; Mondal, S.P. Synergistic effect of silica and pure palm oil on the machining performances of Inconel 690: A study for promoting minimum quantity nano doped-green lubricants. *J. Clean. Prod.* **2020**, *258*, 120755. [CrossRef]
32. Kazeem, R.A.; Fadare, D.A.; Ikumapayi, O.M.; Adediran, A.A.; Aliyu, S.J.; Akinlabi, S.A.; Jen, T.C.; Akinlabi, E.T. Advances in the Application of Vegetable-Oil-Based Cutting Fluids to Sustainable Machining Operations—A Review. *Lubricants* **2022**, *10*, 69. [CrossRef]
33. *ISO 6506-1:2005*; Metallic materials—Brinell hardness test—Part 1: Test method. Available online: https://www.iso.org/standard/37739.html (accessed on 5 July 2023).
34. *ASTM E23-18*; Standard Test Methods for Notched Bar Impact Testing of Metallic Materials. Available online: https://www.astm.org/e0023-18.html (accessed on 5 July 2023).
35. *ISO 3685:1993*; Tool-life testing with single-point turning tools. Available online: https://www.iso.org/standard/9151.html (accessed on 5 July 2023).
36. Altintas, Y. *Manufacturing Automation*, 2nd ed.; Cambridge University Press: Vancouver, BC, Canada, 2012; ISBN 9781107001480.
37. Yeo, C.Y.; Tam, S.C.; Jana, S.; Lau, M.W. A technical review of the laser drilling of aerospace materials. *J. Mater. Process. Technol.* **1994**, *42*, 15–49. [CrossRef]
38. Nakayama, K.; Arai, M. Comprehensive Chip Form Classification Based on the Cutting Mechanism. *CIRP Ann.* **1992**, *41*, 71–74. [CrossRef]
39. Colwell, L.V. Predicting the Angle of Chip Flow for Single-Point Cutting Tools. *ASME-J. Fluids Eng.* **1954**, *76*, 199–203. [CrossRef]

40. Jayal, A.D.; Balaji, A.K. Effects of cutting fluid application on tool wear in machining: Interactions with tool-coatings and tool surface features. *Wear* **2009**, *267*, 1723–1730. [CrossRef]
41. Wood, P.; Díaz-Álvarez, J.; Rusinek, A.; Gunputh, U.; Bahi, S.; Díaz-Álvarez, A.; Miguélez, M.; Lu, Y. Microstructure Effects on the Machinability of AM-Produced Superalloys. *Crystals* **2023**, *13*, 1190. [CrossRef]
42. Boud, F.Ã. Bar diameter as an influencing factor on temperature in turning. *Int. J. Mach. Tools Manuf.* **2007**, *47*, 223–228. [CrossRef]
43. CIMVANTAGE 31-48—Poolsünteetilise Emulsiooni Kontsentraat, 200L. Available online: https://www.venten.ee/cimvantage-31-48-poolsunteetilise-emulsiooni-kontsentraat-200l-13973.html (accessed on 25 August 2023).
44. Mohan, C.B.; Gopalakrishna, K.; Mahesh Lohith, K.S.; Venkatesh, K.; Divakar, C.; Mithun, R.B.; Naveen, T.N. Coolant Lubricity and Coolant-Lube Compatibility with Regard to Slideway Behavior. *J. Braz. Soc. Mech. Sci. Eng* **2008**, *30*, 285–289. [CrossRef]
45. Silliman, J.D. (Ed.) *Cutting and Grinding Fluids: Selection and Application Paperback*, 2nd ed.; Society Manufacturing Engineers: Southfield, MI, USA, 1992; ISBN 978-0872634237.
46. Rossmoore, H. Extending Cutting Fluid Life. *Manuf. Eng.* **1975**, *75*, 27–28.
47. Metalworking fluids – the complete Engineers Guide - Q8Oils. Available online: https://www.q8oils.com/metalworking/engineers-guide/ (accessed on 15 September 2023).
48. Wear, T.; Include, T.; Contamination, T.; Include, T.; Chemistry, T.; Include, T. *FAST Filtration Analysis Services Technology Ltd*; 2017; Volume 44.
49. Eppert, J. Understanding Contamination in Metalworking Fluids-Contamination Part 4. Available online: https://mwfmag.com/?q=content/contamination-part-4 (accessed on 15 September 2023).
50. Byers, J.P. (Ed.) *Metalworking Fluids*; Maecel Dekker: New York, NY, USA, 1994; ISBN 9781498722223.